Ceramics International 43 (2017) 8603–8610

Contents lists available at ScienceDirect

Ceramics International

journal homepage: www.elsevier.com/locate/ceramint

Controllable synthesis of porous C_xN_y nanofibers with enhanced electromagnetic wave absorption property

Tao Zhang[a], Pengyu Zhou[a], Bo Xiao[a], Jian Zhang[a], Guangwu Wen[b], Bo Zhong[a], Long Xia[a,*]

[a] School of Materials Science and Engineering, Harbin Institute of Technology (Weihai), Weihai 264209, PR China
[b] School of Materials Science and Engineering, Shandong University of Technology, Zibo 255049, PR China

ARTICLE INFO

Keywords:
Porous C_xN_y nanofibers
Polyacrylonitrile nanofibers
Microwave absorption

ABSTRACT

Porous C_xN_y nanofibers are controllably synthesized by a simple two-step method. The prepared samples possess uniform micropores and a chemical composition of $C_{0.73}$ $N_{0.27}$ with a surface area of 329 m^2 g^{-1}. The obtained C_xN_y nanofibers exhibit remarkable electromagnetic (EM) wave absorption properties when compared with conventional one-dimensional carbon materials. The minimum reflection loss (RL) reaches −36 dB at 2.7 GHz when the ratio of the C_xN_y absorbent added in paraffin matrix is only 1:3. The bandwidth of the RL below −10 dB covers 7.7 GHz (8.1–15.8 GHz) at the sample thickness of 2.5 mm. A possible EM wave loss mechanism was proposed in detail. The multiple reflection and dielectric loss could govern the excellent EM absorption leading the product to a probable application in stealth materials.

1. Introduction

The wide application of wireless communication terminals, such as laptop, unmanned aerial vehicle and radar, have made people's daily life more convenient and efficient, but at the same time, excessive electromagnetic (EM) radiation also does harm to biological systems, electronic equipment and information safety [1–4]. The increasing radiation problem has therefore attracted much attention by global researchers, and great efforts have been made to eliminate EM pollution. Using EM absorbing materials to eliminate EM wave pollution is practical in both civil and military fields. As is known to all, an excellent EM absorbent should not only have a strong EM absorption and wide frequency bandwidth, but also have a low density with minor dosage in the matrix [5,6]. Magnetic metallic materials, such as iron oxides, nickel and cobalt particles, are commonly used as EM wave absorbents due to their strong absorption and low cost [7,8]. However, the high density of these magnetic particles has strictly limited their application scope, especially in aviation industry.

Recently, there is a growing interest in porous carbon nanofibers for different applications [9–12], such as attenuating EM waves [13,14]. The weight of porous carbon nanofibers is remarkably lighter than magnetic particles, and their porous structures exhibit extremely high surface area, which in turn increases the reflection surfaces for incident EM waves. The porous structure of carbon nanofibers leads to more surface atoms with unsaturated bonds, which is helpful to improve the dielectric loss [15]. According to literatures, different kinds of carbon nanofiber composites have been successfully fabricated, such as graphene/carbon-nanofibers [16,17], carbon-nanofibers/carbon-paper composite [18] and metal oxide-decorated carbon nanofibers [19], which effectively combine the excellent properties of the two components. The prominent high temperature stability, high specific surface area, low density and excellent structure flexibility of carbon nanofibers prove that they would be an ideal candidate for EM wave absorption.

Although various magnetic particle-decorated carbon nanofibers with different EM wave absorbing properties have been reported, to the best of our knowledge, there are still few reports on the controllable fabrication of porous C_xN_y nanofibers as any researchers have reported that doping N atoms on carbon-based materials could effectively enhance their properties in various fields [20–22]. Herein, we provide a simple controllable two-step method for fabricating porous C_xN_y nanofibers, which is schematically displayed in Fig. 1. As shown in Fig. 1, porous C_xN_y nanofibers are fabricated by a simple one-step pyrolysis route using ammonia water as etching reagent. The polar molecules of NH_3 and H_2O would attach on the -CN- pendant groups of the polyacrylonitrile (PAN) nanofibers through the electrostatic coupling. Unlike the reported chemical vapor deposition (CVD) method for synthesizing one-dimensional carbon-based materials which usually needs catalyst to assist the process [23], the preparation of porous C_xN_y nanofibers only use ammonia water as etching reagent, thus making the chemical composition more controllable. Moreover, porous C_xN_y nanofibers are prepared for the first time by using a simple reactive pyrolysis method, which is both efficient and environmental-friendly.

* Corresponding author.
E-mail address: xialonghit@gmail.com (L. Xia).

http://dx.doi.org/10.1016/j.ceramint.2017.03.157
Received 18 January 2017; Accepted 24 March 2017
Available online 27 March 2017

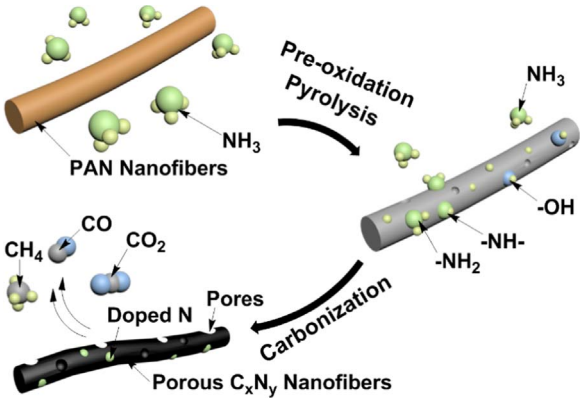

Fig. 1. Sketch map of the one-step fabrication of porous C_xN_y nanofibers.

The as-prepared porous C_xN_y nanofibers exhibit extraordinary EM wave absorption suggesting that the new porous C_xN_y nanofibers could meet the requirement for the next generation of radar stealth materials (light weight, thin thickness, powerful absorption and wide bandwidth) [24].

2. Experimental

2.1. Preparation of porous C_xN_y nanofibers

All chemical reagents in the experiment were analytical grade and used without further purification. Polyacrylonitrile (PAN, 12 g) was dissolved in N, N-dimethylformamide (DMF, 100 mL) to form a transparent homogeneous solution (bright yellow) at room temperature (25 °C). Then, the solution was loaded into an array of syringes and delivered to the tips of metal needles with pressure-assisted pistons (the pressure was controlled at 0.25 MPa). A positive high

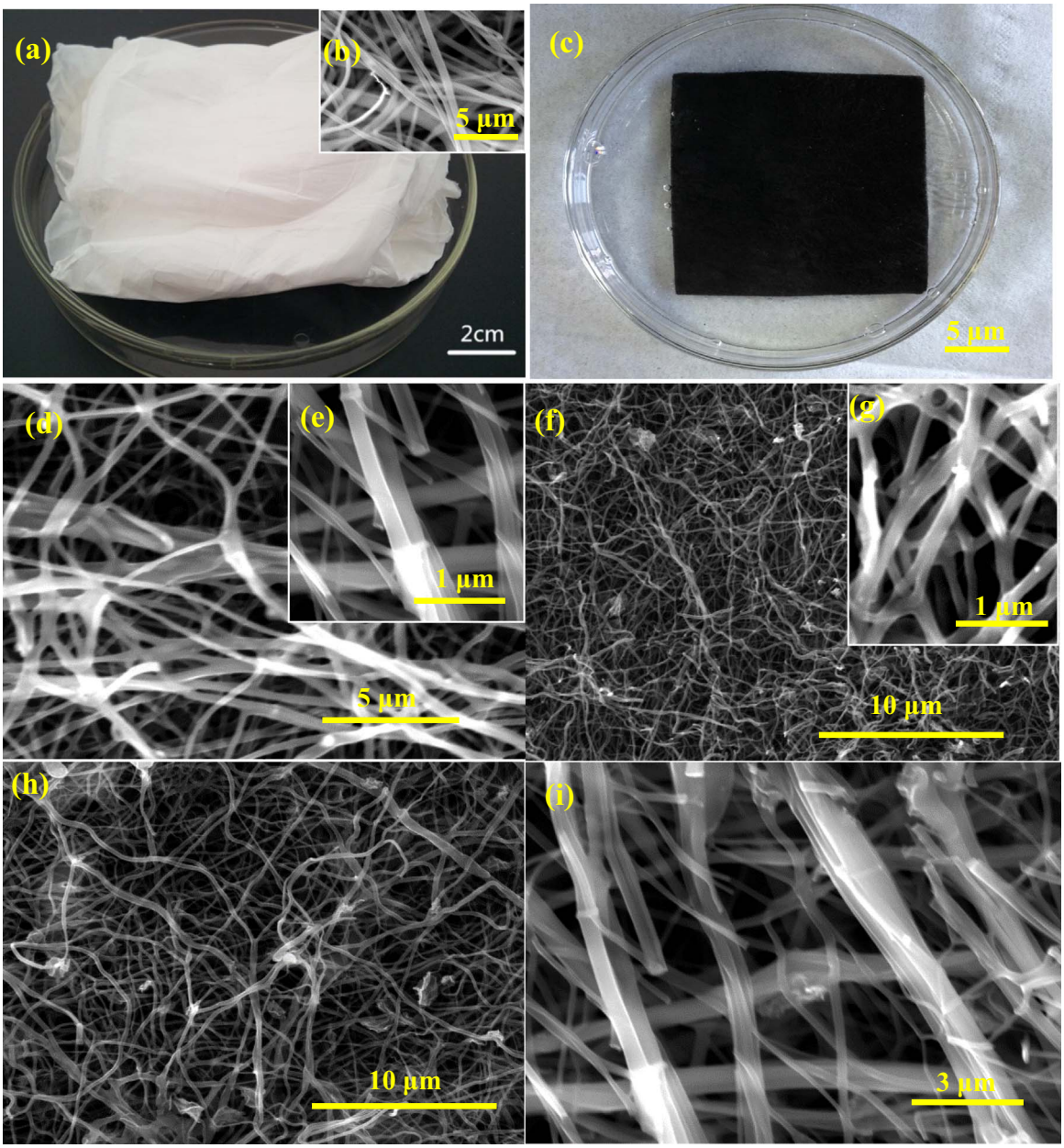

Fig. 2. (a) Digital image of the as-prepared PAN fiber cloth, (b) SEM image of the PAN fibers, (c) Digital image of the annealed C_xN_y nanofibers, (d, e) Low and high magnification SEM images of S1, (f, g) Low and high magnification SEM images of S2, (h, i), Low and high magnification SEM images of S3.

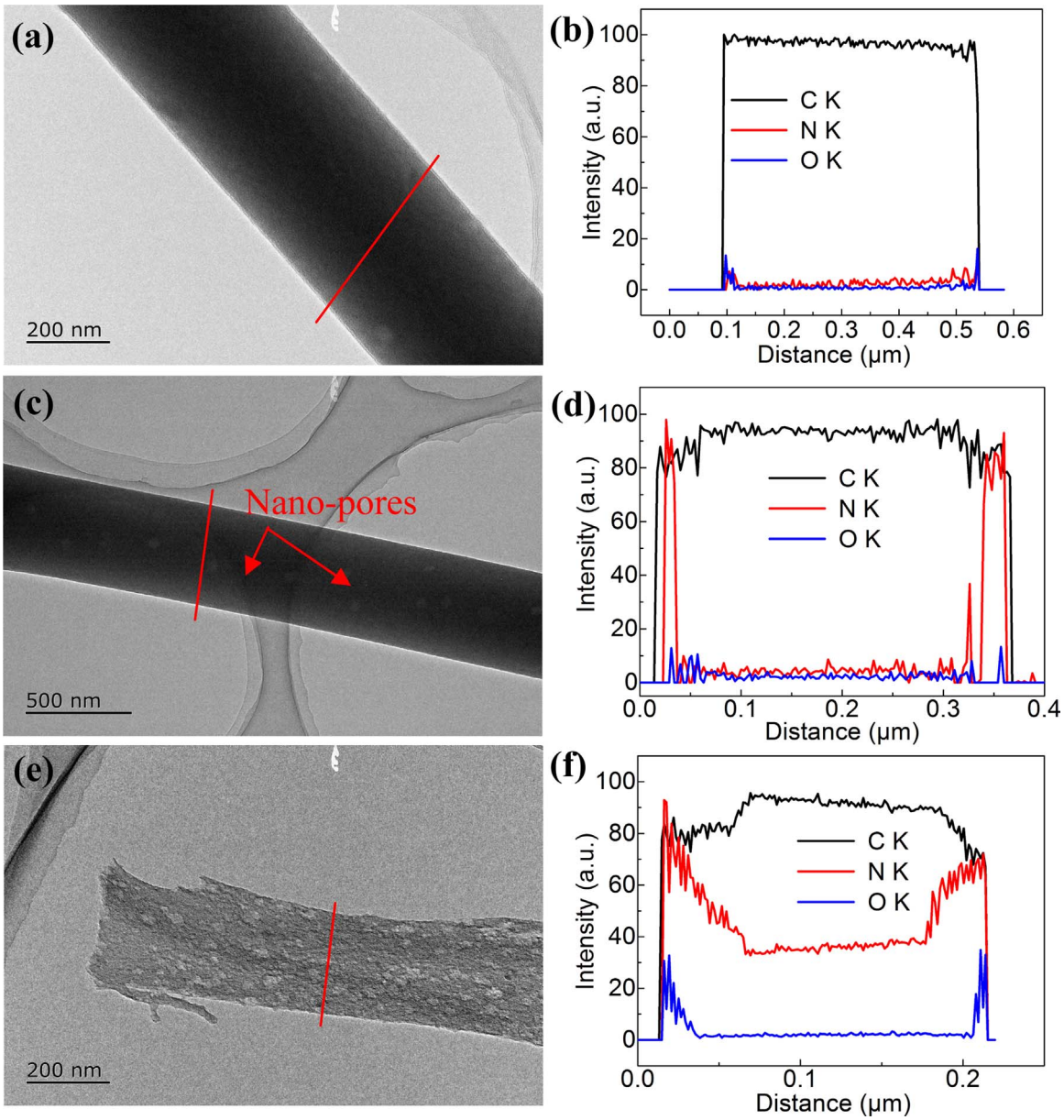

Fig. 3. TEM images and corresponding line-scanning EDS spectra of C_xN_y nanofibers, (a, b) S1, (c, d) S2, (e, f) S3.

voltage of 20 kV was loaded on the suspension via the needles. The batch-production electrospun fibers were collected by an aluminum foil working as ground electrode. After that, pre-oxidation for the product was conducted at 280 °C for 15 min under ambient air before carbonization. Then the fibers were carbonized and etched in a tube furnace at 800–1000 °C in flowing ammonia water (120 mL/min, 0.88 g/cm^3, 32 wt%) carried by nitrogen atmosphere (80 mL/min) for 5–20 min at a heating rate of 3 °C/min. The as-prepared samples obtained at etching temperature of 800 °C for 5 min, 900 °C for 10 min and 1000 °C for 20 min were defined as S1, S2 and S3, respectively.

2.2. Structure characterization

The sample morphologies were characterized by scanning electron microscopy (SEM, MX2600FE) and transmission electron microscopy (TEM, Philips Tecnai F30). The chemical characteristics of the products were examined using X-ray photoelectron spectroscopy (XPS, Physical Electronics PHI 5700 with Mg exciting source). The oxidation behavior of PAN nanofibers was characterized by differential thermal analysis (DTA) and thermogravimetry (TG) (Netzsch STA 409c) from 25 to 400 °C in ambient air at a heating rate of 5 °C/min. The microstructure of the sample was examined by Raman spectroscopy (Renishaw, RM-1000). The Barrett-Emmett-Teller (BET) surface area and pore characteristics were examined by a conventional volumetric method using N_2 at 77 K on Micrometritics ASAP 2020.

2.3. EM wave absorption measurements

EM wave absorption properties of the products were measured based on the Coaxial transmission/reflection method [25]. First, the as-synthesized samples were uniformly mixed with paraffin wax with a mass ratio of 1:3. Then the absorbent/paraffin wax hybrids were introduced into a hollow cylinder with an inner diameter of 3.0 mm, outer diameter of 7.0 mm and the height was about 3 mm. After that, a vector network analyzer (Agilent, N5224A) with transmission reflection mode GHz was operated at room temperature (25 °C) to measure the EM parameters (ε', ε'') of the samples in the range of 2–18 GHz.

According to the transmit-line theory [2,26], the EM wave absorption property of materials can be calculated as follows:

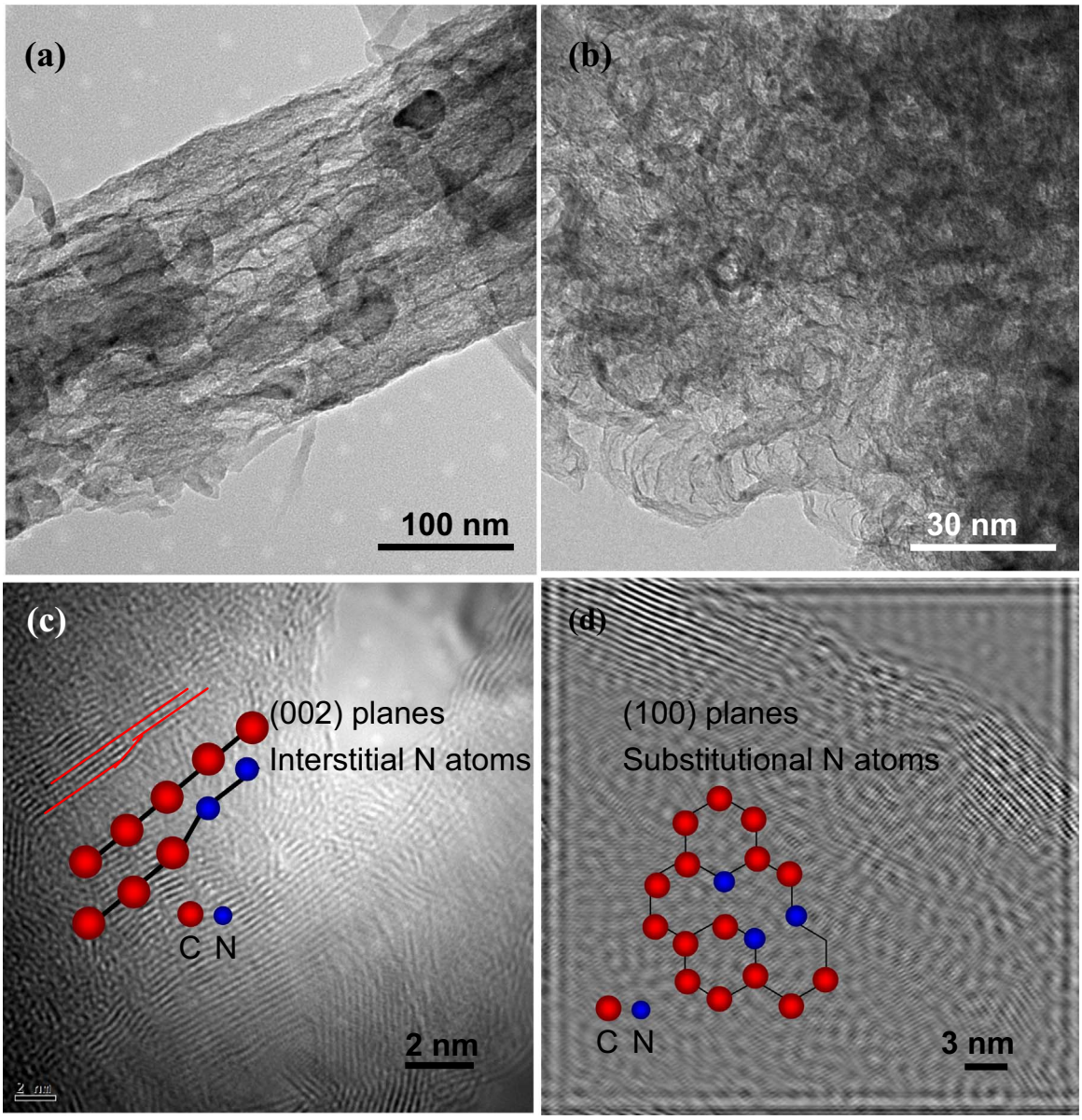

Fig. 4. (a) Low and (b) high magnification TEM images of S3, (c, d) the corresponding HRTEM images of S3 observed at perpendicular directions.

$$Z_i = Z_O(\mu_r/\varepsilon_r)^{1/2} \tanh [j(2\pi fd/c)(\mu_r\varepsilon_r)^{1/2}] \quad (1)$$

$$R_L(dB) = 20 \log \left| \frac{Z_i - Z_0}{Z_i + Z_0} \right| \quad (2)$$

where Z_i is the input impedance of the absorbent, Z_O is the impedance of air, μ_r and ε_r are the relative complex permeability and permittivity, respectively. d is the thickness of the hybrids and c is the velocity of EM waves in free space. f is the frequency of the EM waves, RL (dB) is the reflection loss of the hybrids.

3. Results and discussions

In this paper, the pre-oxidation process at 280 °C is the critical step to preserve the fibrous structure in ambient atmosphere before the carbonization process. If the PAN fibers are directly heated to 800 °C, the original fibers would melt together to form a molten cluster. Fig. 2a and b show digital and SEM images of the PAN fibers. The PAN fibers prepared by electrospinning exhibit cloth-like morphology and are about 400 nm in diameter. The cloth-like structure of the carbonized C_xN_y nanofiber can be observed from the digital image (Fig. 2c). Fig. 2d and e show the SEM images of S1. The fibers exhibit curved and solid morphology with an average diameter of 200 nm after annealing for 5 min Fig. 2f and g display the SEM images of S2. Fig. 2h and i show the SEM images of S3. With the increase of the etching temperature and soaking time, the diameter of fibers drops to around 100 nm (Fig. 2f). The fibers exhibit a semitransparent morphology, which suggests that a large number of carbon atoms could be etched by ammonia water. Although the samples shrink during the carbonization, the fibrous morphology is well preserved in the final products and their diameters are in the range of 100–200 nm.

Fig. 3 shows a group of TEM images and the corresponding EDS line-scanning spectra of the C_xN_y nanofibers heat-treated under different temperatures and time. Fig. 3a shows the TEM image of S1 and the diameter of the sample is about 260 nm. To understand the chemical composition of this sample, an EDS line scan is performed along radial direction. Lines of composition profiles across the surface regions display the profiles of C, N and O. As is shown in Fig. 3b, very few N and O elements are detected from the surface region (in a depth about several nanometers). In contrast, there is relatively high C

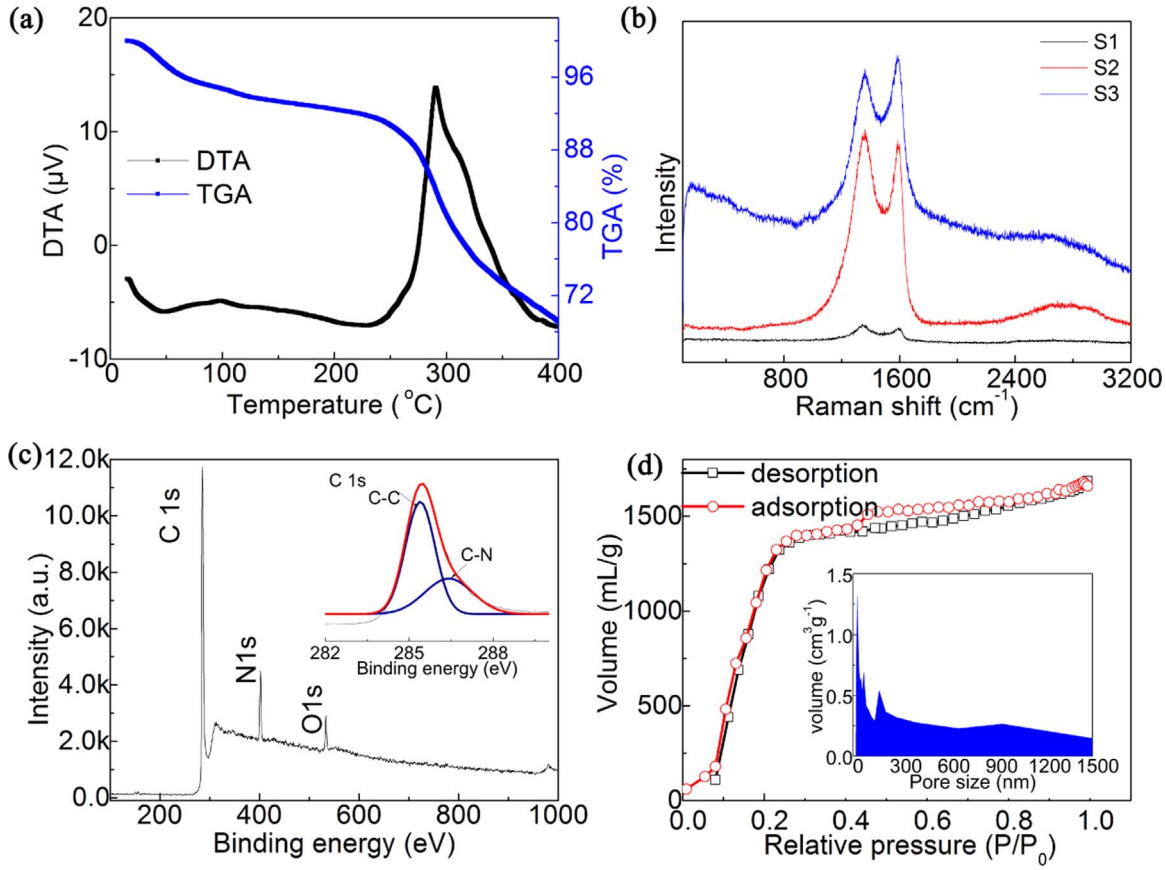

Fig. 5. (a) TGA and DTA spectrum of the PAN nanofibers, (b) Raman spectra of the as-prepared C_xN_y nanofibers samples S1, S2 and S3, (c) XPS spectra of S3, (d) Nitrogen adsorption-desorption isotherm of S3 and the corresponding pore size distribution.

concentration from the surface to the core area, suggesting that the fibers are not sufficiently etched by ammonia water. Fig. 3c shows the TEM image of S2. Some of the nanopores distribute randomly on the fiber surface. From the EDS line scan (Fig. 3d), a certain number of N elements are detected in the surface region (in a depth about 20 nm), but the concentration of O is still low in the fiber. Fig. 3e exhibits the TEM image of S3. The fibers exhibit porous morphology, where the pore size is about 15 nm. The obvious diameter shrink of the fiber treated at a higher annealing temperature and longer etching time could be attributed to the reactions between carbon, NH_3 and active hydrogen decomposed from water [27,28]. The possible reactions are shown in Eqs. (3)–(5). Compared with other samples, S1 exhibits featureless characteristic because of its dense morphology and the relatively high C concentration, which suggests that the fiber is not sufficiently etched by ammonia water. From the line scanning results of EDS of S3 (Fig. 3f), the doping depth of N and O elements expands obviously (in a depth about 80 nm), indicating that the reaction rate of carbon with NH_3 and H is accelerated by higher temperature. The elemental distributions further provide an evidential support regarding the heterogeneous composition of the products.

$$C + 2NH_3 \rightarrow CH_4 + N_2 + H_2 \quad (3)$$

$$C + 2NH_3 \rightarrow CH_4 + 1/2N_2 + H_2 + N\cdot \quad (4)$$

$$C + H\cdot \rightarrow CH_4 \quad (5)$$

To further investigate the pore morphology and crystallite structure of the C_xN_y nanofibers, a group of HRTEM is performed. Fig. 4a and b show the low and high magnification TEM images of S3. The nanopores with a diameter ranging from 4 nm to 60 nm, demonstrating irregular geometry characteristics. A typical HRTEM image of the pores is shown in Fig. 4c which illustrates the clear diffraction fringes corresponding to (002) planes of hexagonal graphite structure. It is interesting to find that a large number of dislocation-like defects are around the pore with an interplanar spacing about 0.322 nm, which is slightly narrower than of the graphite crystal (0.33 nm). This phenomenon attributes to the doping of nitrogen atoms in the carbon lattice. The similar atom size of carbon and nitrogen atoms is a critical condition for the defects [29,30]. The slightly narrower interplanar spacing corresponds to the small atomic radius of nitrogen. Fig. 4d shows the HRTEM image taken in perpendicular direction to the (002) planes. The irregular fractal-like fringes also confirm the existence of line defects in the lattice of the as-prepared C_xN_y nanofibers.

To understand the pyrolysis behavior of the PAN precursor, TGA/DTA was conducted in flowing air from room temperature (25 °C) to 400 °C with a heating rate of 3 °C/min (Fig. 5a). According to the TGA curve, the precursor starts to pyrolyze at about 270 °C and then shows a sharp weight loss from 270 to 400 °C. The final weight loss of the precursor is about 30% at 400 °C. As is shown in the DTA curve, a broad endothermic peak occurs at about 290 °C in virtue of the transformation of PAN to oxynitrides and carbonization [31,32].

Raman spectra of the as-prepared C_xN_y nanofibers record with 488 nm wave length excitation is shown in Fig. 5b. Two strong peaks at 1346 and 1583 cm^{-1} can be clearly observed in the spectra of S1, S2 and S3, respectively. According to previous reports on doped carbon materials, the double peaks at 1346 and 1583 cm^{-1} are attributed to the D and G bands of typical graphitic structure [33]. The D band could be explained by a relaxation of wave vector selection rules, resulting from finite crystallite size effects, which suggests the existence of nitrogen doping in the carbon lattice. The intensity ratios of I_G/I_D are 0.8 (S1), 0.92 (S2) and 1.45 (S3), respectively. The increasing trend indicates that a higher annealing temperature and longer soaking time

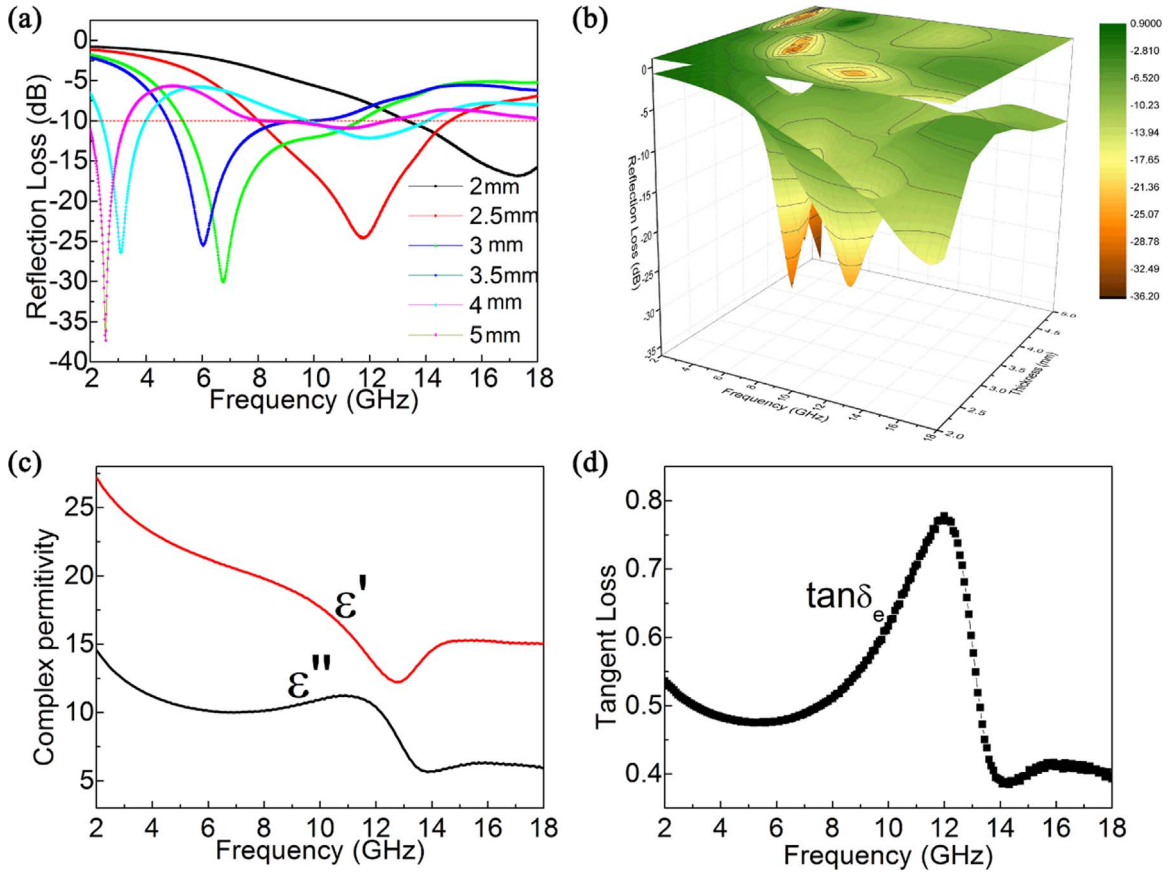

Fig. 6. (a, b) The reflection loss, (c) the complex permittivity, (d) the dielectric tangent loss of the sample at 5 mm of the porous C_xN_y nanofiber sample S3.

Table 1
EM wave absorption properties of materials based on this work and reported one-dimensional carbon composites in recent literatures.

Filter	Type of polymer (used as matrix)	Loading ration (wt%)	Minimum RL (dB)	Thickness (mm) and corresponding effective[a] absorption bandwidth (GHz)		Ref.
C_xN_y nanofibers	Paraffin	20	−36	2.5	7.7	This work
Barium titanate/CNTs[b]	Paraffin	60	−29.6	1.0	1.7	[3]
FeCoNi-filled CNTs	Epoxy	1.3	−28.2	2.0	5.8	[6]
Double-layer Co/La/Ni doped MWCNTs[c]	PVC[d]	7.6	−27.85	4.0	1.6	[14]
$La(NO_3)_3$/Amorphous CNTs	PVC	8.0	−25.02	2.0	5.8	[23]
Carbonyl iron /Carbon nanofiber/ Lanthanum-strontium manganese oxide	Paraffin	30	−8.5	2.0	–	[39]
Porous Carbon Fibers	Epoxy	6	−31	2.3	the whole X-band	[40]
Helical nanofiber-T-ZnO[e] whiskers	Paraffin	10	−15.97	3.0	5.5	[41]

[a] Reflection loss below −10 dB.
[b] Carbon nanotubes.
[c] Multi-wall Carbon nanotubes.
[d] Polyvinylchloride.
[e] Tetrapod-shaped ZnO.

contribute to the growth of graphite crystals. In addition, a higher wave number band at the range of 2475–2922 cm^{-1} can be observed in the spectra of S2 and S3. The broad band is related to high-order lattice structure and could be assigned to the combination of the D and G bands or a 2D overtone similar to the nitrogen doped graphite materials [34]. This phenomenon also agrees well with the result of I_G/I_D (higher annealing temperature would help the growth of crystallitic structure).

The XPS spectrum of full range scanning (Fig. 5c) measured the existence of carbon (285.2 eV), nitride (398.5 eV) and oxygen (545 eV, in virtue of the absorbed H_2O of the sample) in the products. The C:N atomic ratio calculated from the XPS spectrum is about 1:0.37. Thus, the chemical composition of the product is $C_{0.73}$ $N_{0.27}$. A high resolution spectrum of C 1s peak (the inset of Fig. 5c) shows the existence of C–C (284.7 eV) and C–N (285.4 eV) bonds with additional broadening due to the structural disorder and a possible contribution of C–O (286 eV) bonds [35].

Nitrogen adsorption-desorption isotherms were measured to evaluate the surface area of the C_xN_y nanofibers (Fig. 5d). The isothermic curve of S3 is the typical characteristic of microporous solid and could be probably classified as type V isotherms [36]. The isothermic curve still rises above the relative pressure and the surface area calculated from the isotherms is 329 m^2 g^{-1}. The pore size distribution is obtained basing on the presented nitrogen adsorption isotherms (the inset of Fig. 5d), which widely ranges from 2 nm to 1.5 μm, agreeing well with the SEM and TEM results. The microporous volume is formed by intrinsic etching pores and partial coalescence of the C_xN_y nanofibers. The C_xN_y nanofibers can be easily prepared at the moderate tempera-

ture (800–1000 °C), which is easier than the reported nitrogen doped carbon porous structures [37]. These porous structure of C_xN_y nanofibers is effective in EM wave absorption attenuation.

The EM wave absorbing performance of C_xN_y nanofiber sample S3 is shown in Fig. 6. To evaluate the EM wave absorption of the porous C_xN_y nanofibers, the mixtures containing 25 wt% of C_xN_y nanofiber S3 with paraffin matrix were pressed into toroidal samples with outer diameters of 7.0 mm and inner diameters of 3.0 mm, respectively. The samples were measured at room temperature in the frequency range of 2–18 GHz and the RL can be investigated by equitation (1) and (2), based on which the RL value of an absorbent below −10 dB indicates that 90% of EM energy has been attenuated. If the RL is below −20 dB, 99% of the EM energy is attenuated and the materials are of enhanced absorption properties. Fig. 6a and b show the RL of the C_xN_y nanofibers (S3)/paraffin hybrids as a function of frequency with different thickness. It can be seen that the hybrids are of effective absorbing intensity and bandwidth as most of the RL is below −10 dB. The RL peaks shift from high to low frequency with the increase of sample thickness, and the RL becomes stronger. The minimum RL reaches −38 dB at 2.6 GHz and the absorption band below −10 dB covers from 2 GHz to 12.5 GHz, indicating its feasible application as stealth materials of both S, C, X and KU-bands [38].

To compare the EM absorption property, some reported typical one-dimensional carbon absorbents are listed in Table 1.

Fig. 6c and d shows the complex permittivity and dielectric tangent loss ($\tan\delta_\varepsilon=\varepsilon''/\varepsilon'$) of the composite versus frequency. The real permittivity (ε') presents the storage ability of EM energy and the imaginary part (ε'') of complex permittivity exhibits the electric energy loss [42]. As can be seen, the ε' and ε'' of the composites both decline with the increase of frequency, which can be explained by Debye's equations [43],

$$\varepsilon' = \varepsilon_\infty + \frac{\varepsilon_s - \varepsilon_\infty}{1 + \omega^2\tau^2} \tag{6}$$

$$\varepsilon'' = \frac{(\varepsilon_s - \varepsilon_\infty)\omega\tau}{1 + \omega^2\tau^2} \tag{7}$$

where ε_s is the static permittivity, ε_∞ is the relative dielectric permittivity at the high frequency limit, ω is the angular frequency and τ is the polarization relaxation time. In addition, the decrease of ε' and ε'' as a function of frequency is defined as frequency dispersion [44], which could help to improve the impedance matching condition between the C_xN_y nanofibers and the ambient air.

The excellent EM wave absorption of the as-prepared C_xN_y nanofibers could be mainly controlled by the dielectric loss of the EM waves, resulting form the doping of N atoms in the carbon structure. Pure carbon nanofibers are electrically conductive due to their graphite-layered structure, which has minor contribution to the attenuation of the incident EM waves [45]. After the chemical reactions between carbon nanofibers and the ammonia water according to Eqs. (3)–(5), these dense nanofibers are etched by NH_3 and H_2O, forming a number of nanopores in which N atoms take the place of C atoms. According to the literature, these pores could act as resonant chambers for reflect the EM waves, which benefit the porous structure from achieving enhanced EM wave absorption properties [44]. N doping atoms build C-N covalent bonds with neighboring C atoms, leaving lone pair electrons on the pore surface. The doping of N atoms also changes the lattice structure of graphitic structure as well as its electronic structure. As a result, the dielectric properties of C_xN_y nanofibers could be effectively improved. Moreover, the N doping atoms in graphitic lattice would polarize the covalent C–C bonds, forming an electron-rich interface on the pore surfaces, which could be designated as the polarized center (the effect of polarization relaxation). In addition, the multiple reflections of microwaves between single nanofiber could also help to attenuate the EM energy (if the incident and reflected waves are out of phase by 180°, these two waves would be completely canceled out by each other, thus enhancing the EM wave absorption of the C_xN_y nanofibers) [40].

4. Conclusion

In this paper, the C_xN_y nanofibers are prepared by a simple carbonization process using PAN nanofibers as raw material and ammonia water as etching agent. The products have a chemical composition of $C_{0.73}$ $N_{0.27}$ with a surface area of 329 $m^2\,g^{-1}$ and exhibit excellent EM wave absorbing property (the minimum RL reaches −36 dB at 2.7 GHz and the bandwidth for the RL below −10 dB covers 7.7 GHz). The existence of N atoms in carbon nanofibers could enhance the EM wave absorption. The possible EM wave absorption mechanism was proposed and the C_xN_y nanofibers could be applied as high performance stealth materials.

Acknowledgement

This work was supported by National Natural Science Foundation of China (51302049, 51372052 and 51302050), Project of Natural Scientific Research Innovation Foundation in Harbin Institute of Technology (HIT. NSRIF. 2015106, HIT. ICRST. 2014129) and Technology Development Program at Weihai (2013DXGJ12).

References

[1] M. Han, X. Yin, W. Duan, S. Ren, L. Zhang, L. Cheng, Hierarchical graphene/SiC nanowire networks in polymer-derived ceramics with enhanced electromagnetic wave absorbing capability, J. Eur. Ceram. Soc. 36 (2016) 2695–2703.
[2] D. Sun, Q. Zou, G. Qian, C. Sun, W. Jiang, F. Li, Controlled synthesis of porous Fe_3O_4-decorated graphene with extraordinary electromagnetic wave absorption properties, Acta Mater. 61 (2013) 5829–5834.
[3] G.J.H. Melvin, Q.-Q. Ni, T. Natsuki, Electromagnetic wave absorption properties of barium titanate/carbon nanotube hybrid nanocomposites, J. Alloy. Compd. 615 (2014) 84–90.
[4] S. Senapati, S.K. Srivastava, S.B. Singh, A.R. Kulkarni, SERS active Ag encapsulated Fe@SiO_2 nanorods in electromagnetic wave absorption and crystal violet detection, Environ. Res. 135 (2014) 95–104.
[5] F.M. Idris, M. Hashim, Z. Abbas, I. Ismail, R. Nazlan, I.R. Ibrahim, Recent developments of smart electromagnetic absorbers based polymer-composites at gigahertz frequencies, J. Magn. Magn. Mater. 405 (2016) 197–208.
[6] R. Lv, F. Kang, J. Gu, X. Gui, J. Wei, K. Wang, D. Wu, Carbon nanotubes filled with ferromagnetic alloy nanowires: lightweight and wide-band microwave absorber, Appl. Phys. Lett. 93 (2008) 223105.
[7] J. Wei, J. Liu, S. Li, Electromagnetic and microwave absorption properties of Fe_3O_4 magnetic films plated on hollow glass spheres, J. Magn. Magn. Mater. 312 (2007) 414–417.
[8] Y.-J. Chen, F. Zhang, G.-g. Zhao, X.-y. Fang, H.-B. Jin, P. Gao, C.-L. Zhu, M.-S. Cao, G. Xiao, Synthesis, multi-nonlinear dielectric resonance, and excellent electromagnetic absorption characteristics of Fe_3O_4/ZnO core/shell nanorods, J. Phys. Chem. C 114 (2010) 9239–9244.
[9] J.K. Chinthaginjala, J.H. Bitter, L. Lefferts, Thin layer of carbon-nano-fibers (CNFs) as catalyst support for fast mass transfer in hydrogenation of nitrite, Appl. Catal. A: Gen. 383 (2010) 24–32.
[10] G. Veerappan, W. Kwon, S.-W. Rhee, Carbon-nanofiber counter electrodes for quasi-solid state dye-sensitized solar cells, J. Power Sources 196 (2011) 10798–10805.
[11] N. Jarrah, J.G. van Ommen, L. Lefferts, Development of monolith with a carbon-nanofiber-washcoat as a structured catalyst support in liquid phase, Catal. Today 79–80 (2003) 29–33.
[12] I. Jo, S. Cho, H. Kim, B.M. Jung, S.-K. Lee, S.-B. Lee, Titanium dioxide coated carbon nanofibers as a promising reinforcement in aluminum matrix composites fabricated by liquid pressing process, Scr. Mater. 112 (2016) 87–91.
[13] N. Lu, C. Shao, X. Li, F. Miao, K. Wang, Y. Liu, CuO nanoparticles/nitrogen-doped carbon nanofibers modified glassy carbon electrodes for non-enzymatic glucose sensors with improved sensitivity, Ceram. Int. 42 (2016) 11285–11293.
[14] C. Hou, T. Li, T. Zhao, W. Zhang, Y. Cheng, Electromagnetic wave absorbing properties of carbon nanotubes doped rare metal/pure carbon nanotubes double-layer polymer composites, Mater. Des. 33 (2012) 413–418.
[15] K. Mizuno, J. Ishii, H. Kishida, Y. Hayamizu, S. Yasuda, D.N. Futaba, M. Yumura, K. Hata, A black body absorber from vertically aligned single-walled carbon nanotubes, Proc. Natl. Acad. Sci. USA 106 (2009) 6044–6047.
[16] Y. Cao, P. Li, J. Zhou, Z. Sui, X. Zhou, Hydrodynamics and mass transfer in carbon-nanofiber/graphite-felt composite under two phase flow conditions, Chem. Eng. Process.: Process Intensif. 50 (2011) 1108–1114.
[17] M.M. Shokrieh, M. Esmkhani, A.R. Haghighatkhah, Z. Zhao, Flexural fatigue behavior of synthesized graphene/carbon-nanofiber/epoxy hybrid nanocomposites, Mater. Des. (1980–2015) 62 (2014) 401–408.

[18] X. Li, Y. Tuo, H. Jiang, X. Duan, X. Yu, P. Li, Engineering Pt/carbon-nanofibers/carbon-paper composite towards highly efficient catalyst for hydrogen evolution from liquid organic hydride, Int. J. Hydrog. Energy 40 (2015) 12217–12226.
[19] Z.K. Ghouri, N.A.M. Barakat, M. Obaid, J.H. Lee, H.Y. Kim, Co/CeO_2-decorated carbon nanofibers as effective non-precious electro-catalyst for fuel cells application in alkaline medium, Ceram. Int. 41 (2015) 2271–2278.
[20] X. Deng, Y. Wu, J. Dai, D. Kang, D. Zhang, Electronic structure tuning and band gap opening of graphene by hole/electron codoping, Phys. Lett. A 375 (2011) 3890–3894.
[21] B.G. Sumpter, V. Meunier, J.M. Romo-Herrera, E. Cruz-Silva, D.A. Cullen, H. Terrones, D.J. Smith, M. Terrones, Nitrogen-mediated carbon nanotube growth: diameter reduction, metallicity, bundle dispersability, and bamboo-like structure formation, ACS Nano 1 (2007) 369–375.
[22] X. Wang, X. Li, L. Zhang, Y. Yoon, P.K. Weber, H. Wang, J. Guo, H. Dai, N-doping of graphene through electrothermal reactions with ammonia, Science 324 (2009) 768.
[23] T. Zhao, C. Hou, H. Zhang, R. Zhu, S. She, J. Wang, T. Li, Z. Liu, B. Wei, Electromagnetic wave absorbing properties of amorphous carbon nanotubes, Sci. Rep. 4 (2014) 5619.
[24] F. Qin, C. Brosseau, A review and analysis of microwave absorption in polymer composites filled with carbonaceous particles, J. Appl. Phys. 111 (2012) 061301.
[25] H. Yang, T. Ye, Y. Lin, J. Zhu, F. Wang, Microwave absorbing properties of the ferrite composites based on graphene, J. Alloy. Compd. 683 (2016) 567–574.
[26] P.A. Miles, W.B. Westphal, A. Von Hippel, Dielectric spectroscopy of ferromagnetic semiconductors, Rev. Mod. Phys. 29 (1957) 279–307.
[27] H.P. Boehm, G. Mair, T. Stoehr, A.R. De Rincón, B. Tereczki, Carbon as a catalyst in oxidation reactions and hydrogen halide elimination reactions, Fuel 63 (1984) 1061–1063.
[28] U. Świetlik, B. Grzyb, K. Torchała, G. Gryglewicz, J. Machnikowski, High temperature ammonia treatment of pitch particulates and fibers for nitrogen enriched microporous carbons, Fuel Process. Technol. 119 (2014) 211–217.
[29] M.-G. Jeong, M. Islam, H.L. Du, Y.-S. Lee, H.-H. Sun, W. Choi, J.K. Lee, K.Y. Chung, H.-G. Jung, Nitrogen-doped carbon coated porous silicon as high performance anode material for lithium-ion batteries, Electrochim. Acta 209 (2016) 299–307.
[30] L. Li, L. Gong, Y.-X. Wang, Q. Liu, J. Zhang, Y. Mu, H.-Q. Yu, Removal of halogenated emerging contaminants from water by nitrogen-doped graphene decorated with palladium nanoparticles: experimental investigation and theoretical analysis, Water Res. 98 (2016) 235–241.
[31] N. Yusof, A.F. Ismail, Post spinning and pyrolysis processes of polyacrylonitrile (PAN)-based carbon fiber and activated carbon fiber: a review, J. Anal. Appl. Pyrolysis 93 (2012) 1–13.
[32] P. Musiol, P. Szatkowski, M. Gubernat, A. Weselucha-Birczynska, S. Blazewicz, Comparative study of the structure and microstructure of PAN-based nano- and micro-carbon fibers, Ceram. Int. 42 (2016) 11603–11610.
[33] C.Y. Zhi, X.D. Bai, E.G. Wang, Raman characterization of boron carbonitride nanotubes, Appl. Phys. Lett. 80 (2002) 3590–3592.
[34] H. Chen, Q. Li, N. Teng, D. Long, C. Ma, Y. Wei, J. Wang, L. Ling, Simultaneous micropore development and nitrogen doping of ordered mesoporous carbons for enhanced supercapacitor and Li-S cathode performance, Electrochim. Acta 214 (2016) 231–240.
[35] X. Li, H. Wang, J.T. Robinson, H. Sanchez, G. Diankov, H. Dai, Simultaneous nitrogen doping and reduction of graphene oxide, J. Am. Chem. Soc. 131 (2009) 15939–15944.
[36] K.S.W. Sing, D.H. Everett, R.A.W. Haul, L. Moscou, R.A. Pierotti, J. Rouquerol, T. Siemieniewska, Reporting physisorption data for gas solid systems with special reference to the determination of surface-area and porosity (recommendations 1984), Pure Appl. Chem. 57 (1985) 603–619.
[37] C. Wang, Y. Huang, H. Pan, J. Jiang, X. Yang, Z. Xu, H. Tian, S. Han, D. Wu, Nitrogen-doped porous carbon/graphene aerogel with much enhanced capacitive behaviors, Electrochim. Acta 215 (2016) 100–107.
[38] X. Huang, X. Yan, L. Xia, P. Wang, Q. Wang, X. Zhang, B. Zhong, H. Zhao, G. Wen, A three-dimensional graphene/Fe_3O_4/carbon microtube of sandwich-type architecture with improved wave absorbing performance, Scr. Mater. 120 (2016) 107–111.
[39] S.S.S. Afghahi, A. Mirzazadeh, M. Jafarian, Y. Atassi, A new multicomponent material based on carbonyl iron/carbon nanofiber/lanthanum–strontium–manganite as microwave absorbers in the range of 8–12 GHz, Ceram. Int. 42 (2016) 9697–9702.
[40] G. Li, T. Xie, S. Yang, J. Jin, J. Jiang, Microwave absorption enhancement of porous carbon fibers compared with carbon nanofibers, J. Phys. Chem. C 116 (2012) 9196–9201.
[41] X. Jian, X. Chen, Z. Zhou, G. Li, M. Jiang, X. Xu, J. Lu, Q. Li, Y. Wang, J. Gou, D. Hui, Remarkable improvement in microwave absorption by cloaking a micro-scaled tetrapod hollow with helical carbon nanofibers, Phys. Chem. Chem. Phys. 17 (2015) 3024–3031.
[42] W. Zhou, X. Hu, X. Bai, S. Zhou, C. Sun, J. Yan, P. Chen, Synthesis and electromagnetic, microwave absorbing properties of core–shell Fe_3O_4–poly (3, 4-ethylenedioxythiophene) microspheres, ACS Appl. Mater. Interfaces 3 (2011) 3839–3845.
[43] K.S. Cole, R.H. Cole, Dispersion and absorption in dielectrics I. alternating current characteristics, J. Chem. Phys. 9 (1941) 341–351.
[44] N. Tang, W. Zhong, C. Au, Y. Yang, M. Han, K. Lin, Y. Du, Synthesis, microwave electromagnetic, and microwave absorption properties of twin carbon nanocoils, J. Phys. Chem. C 112 (2008) 19316–19323.
[45] G.S. Park, J.-S. Lee, S.T. Kim, S. Park, J. Cho, Porous nitrogen doped carbon fiber with churros morphology derived from electrospun bicomponent polymer as highly efficient electrocatalyst for Zn–air batteries, J. Power Sources 243 (2013) 267–273.